Supporting Information

MXene-based multifunctional smart fibers for wearable and portable-electronics

Leiqiang Qin,*[a] Jianxia Jiang,[a,b] Lintao Hou,[c] Fengling Zhang[a] and Johanna Rosen*[a]

[a] Department of Physics, Chemistry and Biology (IFM), Linköping University, Linköping, SE-58183, Sweden. E-mail: leiqiang.qin@liu.se; Johanna.rosen@liu.se

[b] Flexible Electronics Innovation Institute, Jiangxi Science and Technology Normal University, Nanchang, 330013, China.

[c] Guangzhou Key Laboratory of Vacuum Coating Technologies and New Energy Materials, Physics Department, Jinan University, Guangzhou, 510632, China.

The gravimetric capacitance from the cyclic voltammetry data is determined from the following equation (1):

$$C = \frac{1}{\Delta V}\int \frac{jdV}{s} \qquad (1)$$

C is the normalized capacitance (in units of F g^{-1}), j is the current density (in A g^{-1}), s is the rate (in V s^{-1}), V is the voltage (in V), ΔV is the voltage window (in V).

In order to achieve optimal performance with asymmetric supercapacitors, there should be a charge balance between the positive and negative electrodes. The mass ratio of positive and negative electrodes is determined by using the charge balance theory as follows:

$$q = C \times V \times m \qquad (2)$$

where C, V and m are specific capacitance, potential range and mass of the active material, respectively. To attain the charge balance, the following condition must be satisfied

$$q_+ = q_- \qquad (3)$$

$$\frac{m_+}{m_-} = \frac{C_+ \times V_+}{C_- \times V_-} \qquad (4)$$

The energy density of the device is obtained from the formula given in Equation (5):

$$E = \frac{1}{2} \times C_{device}^{gravimetric} \times \frac{(\Delta V)^2}{3600} \qquad (5)$$

where E is the energy density (in Wh/g), $C_{device}^{gravimetric}$ is the gravimetric capacitance obtained from Equation (1) and ΔV is the discharge voltage range (in volts, V).

The power density of the device is calculated from the formula given in Equation (6):

$$P = \frac{E}{\Delta t} \times 3600 \qquad (6)$$

where P is the power density (in W/g), E is the gravimetric energy density obtained from Equation (5) and Δt is the discharge time (in seconds, s).

The ion-diffusion mechanism in the fibers was investigated by analyzing the function curves of peak current (i_p) against scan rate (v) from the cyclic voltammograms, following the power law dependence of i_p on v, $i_p = av^b$, where a and b are adjustable parameters. The value of b provides

important insights into the charge-storage kinetics: when b is close to 1, it indicates a high-rate capacitive storage mechanism, and b $\approx$ 0.5 is the signature of slow semi-infinite diffusion.

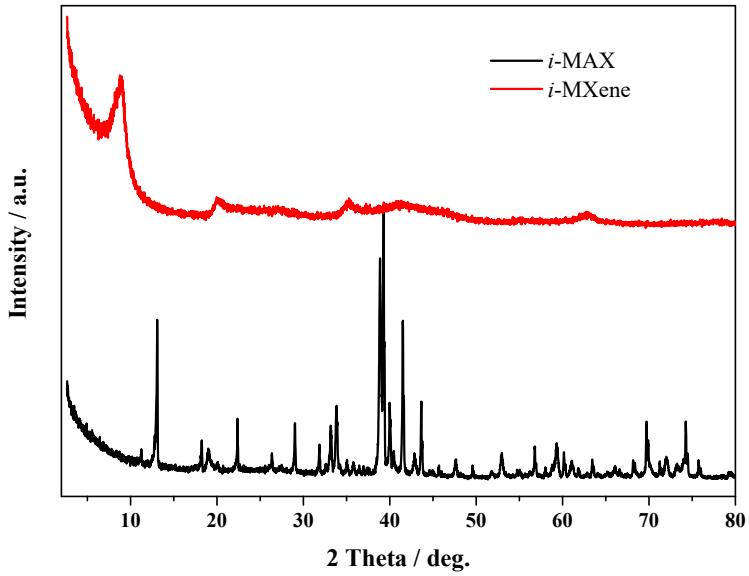

Fig. S1. XRD pattern of *i*-MAX phase and *i*-MXene.

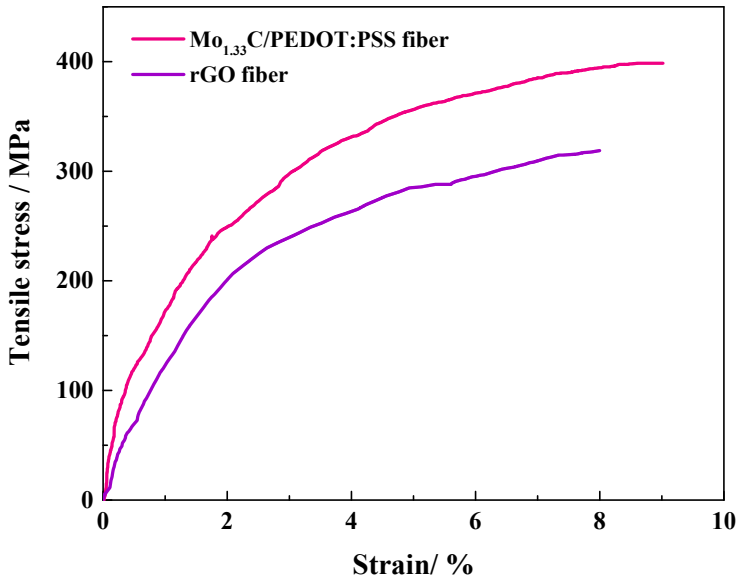

Fig. S2. Typical stress-strain curves of $Mo_{1.33}C$/PEDOT:PSS fiber and rGO fiber.

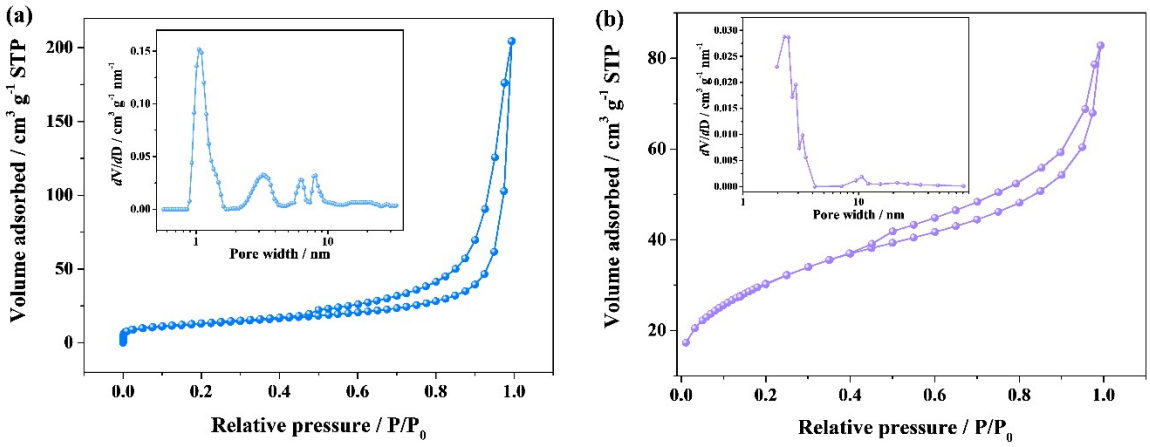

Figure S3. N_2 adsorption-desorption isotherms (STP, standard temperature and pressure) of $Mo_{1.33}C$/PEDOT:PSS fiber (a) and rGO fiber (b). The inset is their corresponding pore-size distribution.

N_2 adsorption-desorption measurements confirm the porosity of the $Mo_{1.33}C$ /PEDOT:PSS fiber and rGO fiber. The $Mo_{1.33}C$/PEDOT:PSS fiber exhibited a micropore-dominated pore-size distribution (Fig. S3 a), while rGO fiber showed a pore size distribution dominated by mesopores.

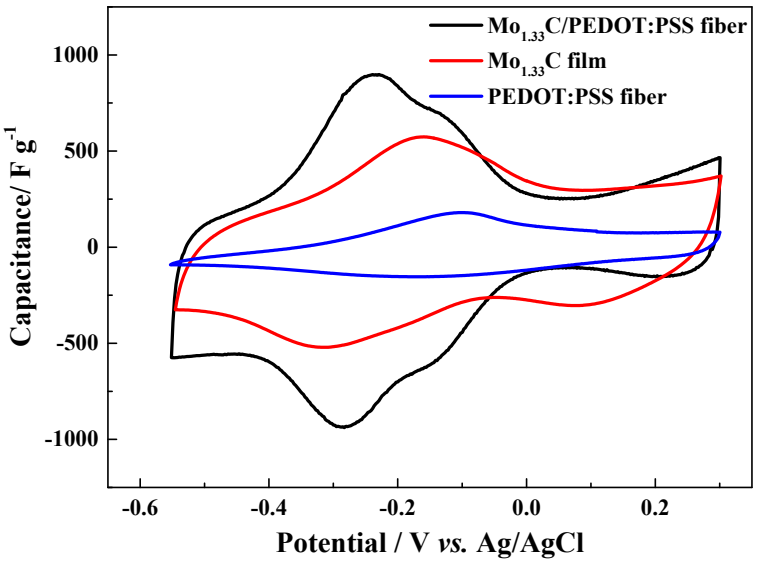

Fig. S4. The cyclic voltammograms of pristine $Mo_{1.33}C$ film, PEDOT:PSS fiber and $Mo_{1.33}C$ /PEDOT:PSS hybrid fiber at scan rate 50 mV s^{-1} for compare the electrochemical performance. The fibers of $Mo_{1.33}C$ could not be prepared using the method in this work. The electrochemical performance of pristine $Mo_{1.33}C$ film was used to instead the $Mo_{1.33}C$ fibers.

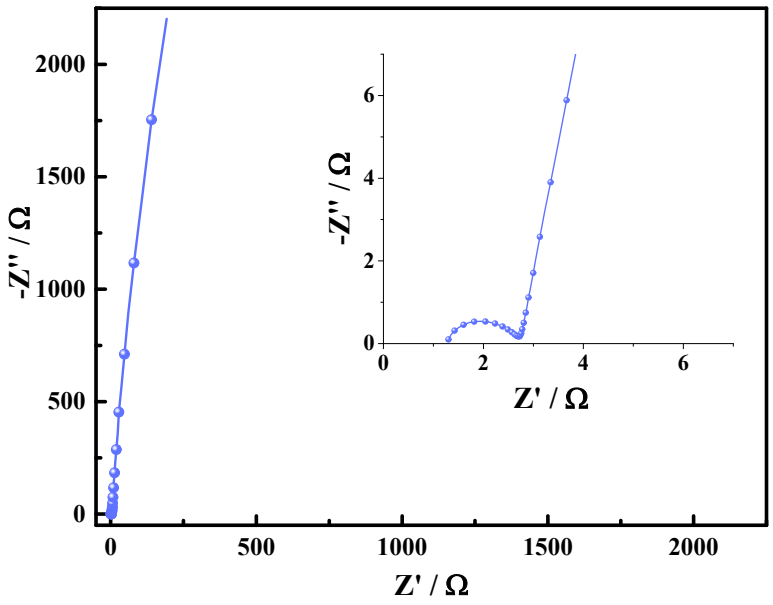

Fig. S5. The Nyquist plot of a hybrid fiber electrode in 3 м H_2SO_4.

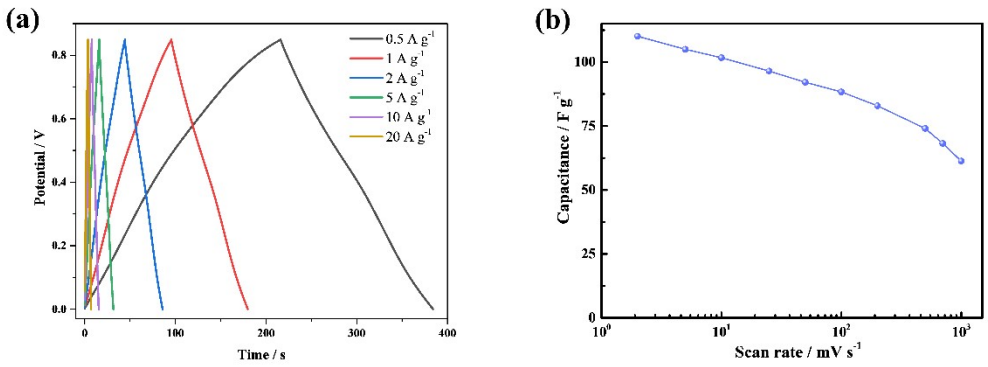

Fig. S6. a) Galvanostatic charge-discharge (GCD) curves of a symmetrical fiber type supercapacitor at different current densities. b) Capacitance of a symmetrical fiber type supercapacitor as a function of scan rate.

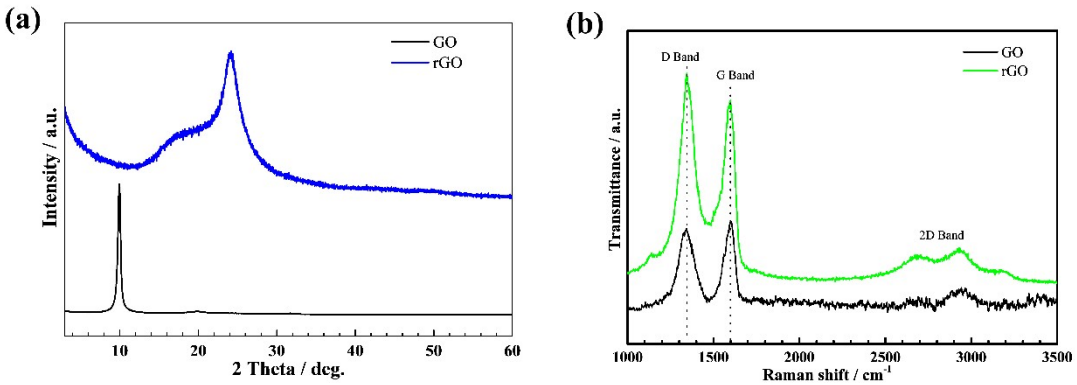

Fig. S7. XRD (a) and Raman (b) spectra of GO and rGO fiber.

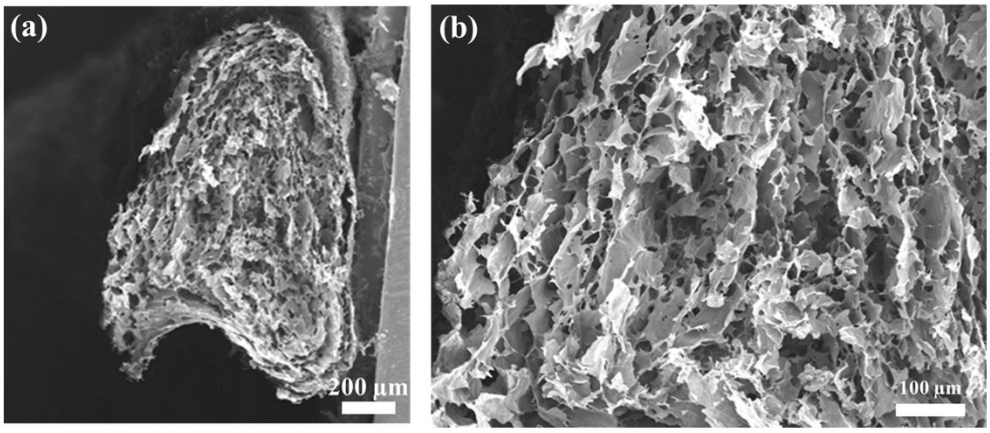

Fig. S8. SEM image of a cross-section of a hybrid fiber at different magnifications.

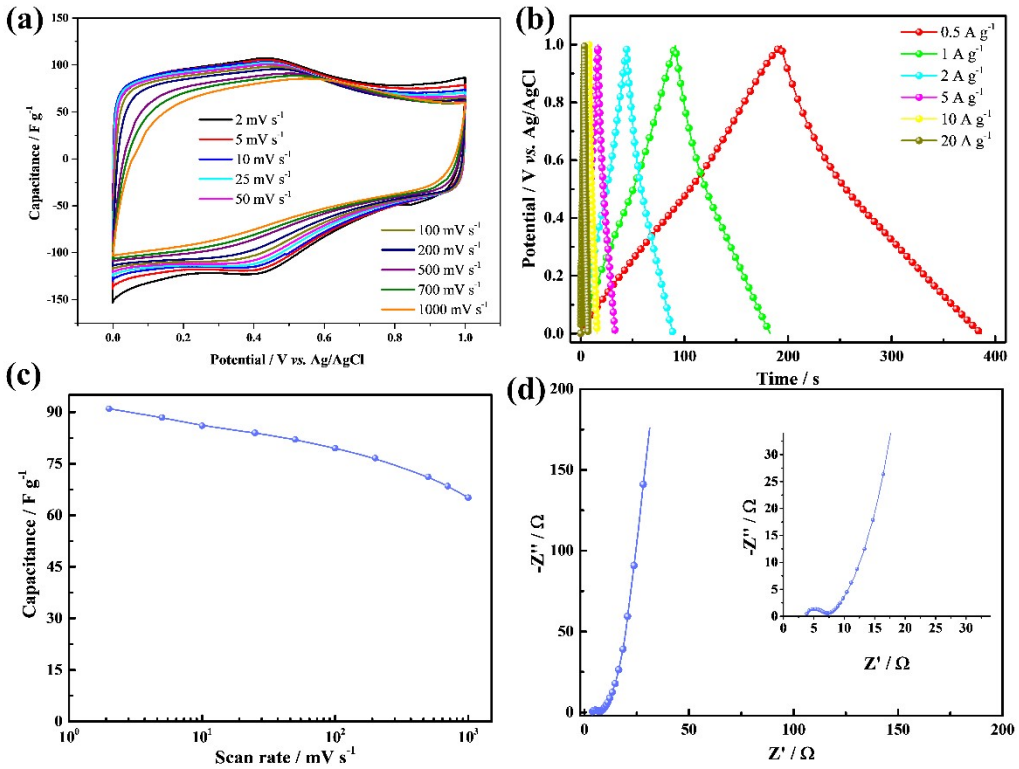

Fig. S9. Electrochemical performance of rGO fiber electrodes. a) CV curves of rGO fiber electrodes at different scan rates. b) Galvanostatic charge-discharge (GCD) curves of fiber electrodes at different current densities. c) Capacitance of fiber electrodes as a function of scan rate. d) EIS curve of rGO fiber electrode.

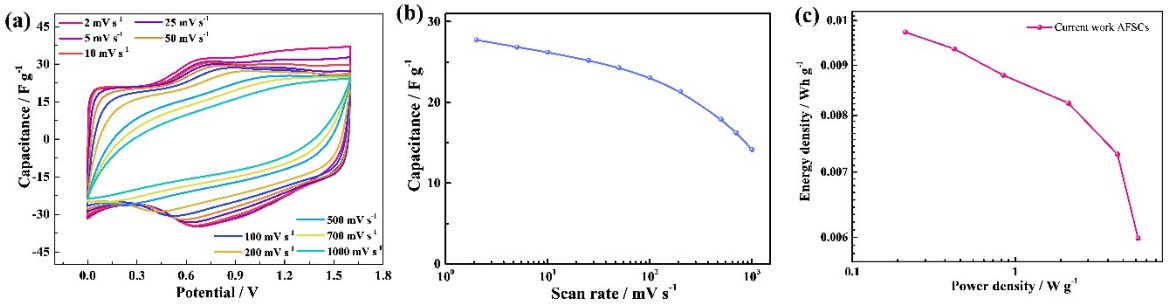

Fig. S10. Electrochemical performance of asymmetric fiber type supercapacitors (AFSCs) considering electrolytes developed using MXene-based fibers as cathodes and rGO fibers as anode. a) CV curves of $Mo_{1.33}C$/PEDOT:PSS//rGO fiber-based supercapacitors at different scan rate. b) Scan rate dependent capacitance of AFSCs. c) Plot of energy density versus power density for AFSCs.

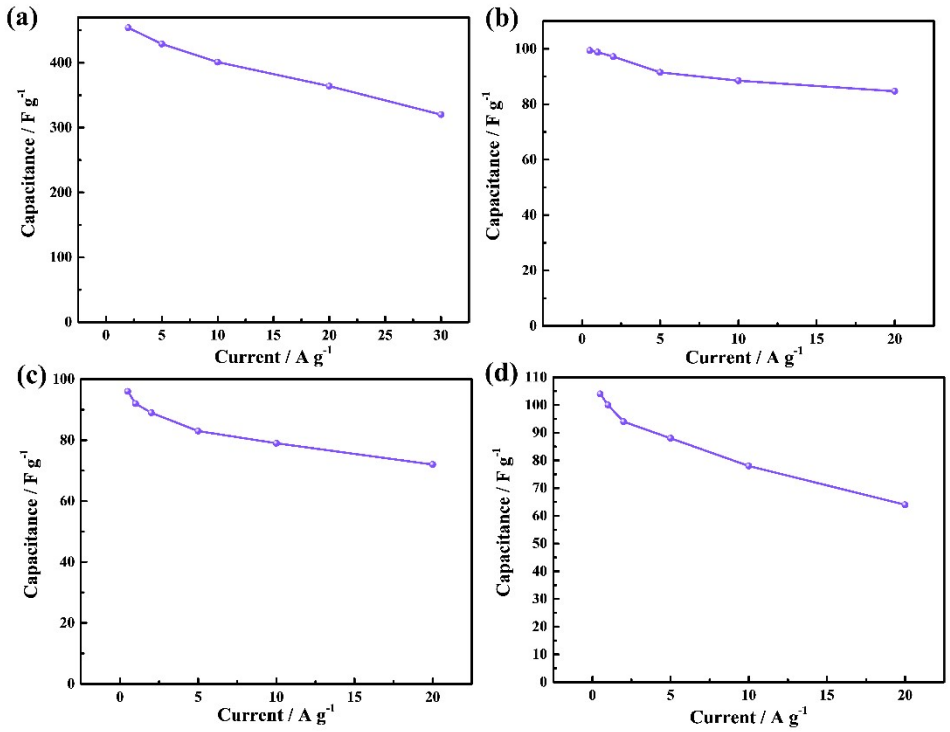

Fig. S11. The specific capacitance curves of $Mo_{1.33}C$ /PEDOT:PSS hybrid fiber in 3 M H_2SO_4 (a), $Mo_{1.33}C$ /PEDOT:PSS hybrid fiber based symmetrical supercapacitors (b), rGO fiber based symmetrical supercapacitors (c) and $Mo_{1.33}C$ /PEDOT:PSS//rGO fiber-based Supercapacitors (d) calculated from GCD.

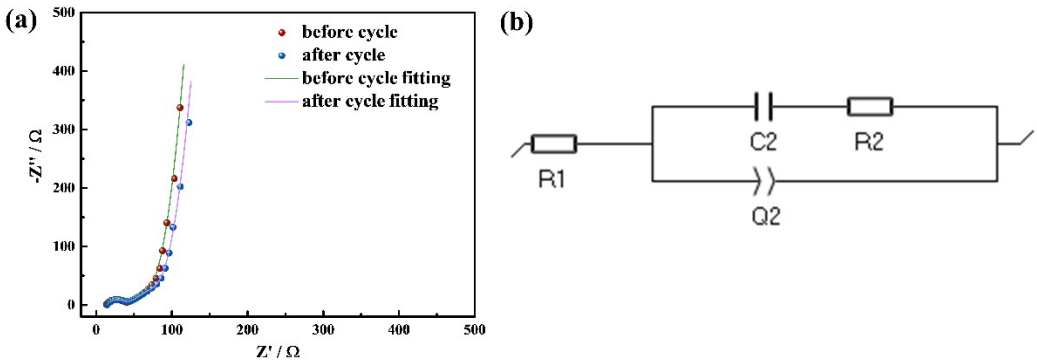

Fig. S12. (a) EIS and corresponding fitted curves of asymmetric fiber type supercapacitors before and after the cycling test. (b) The equivalent circuit using for fitting.

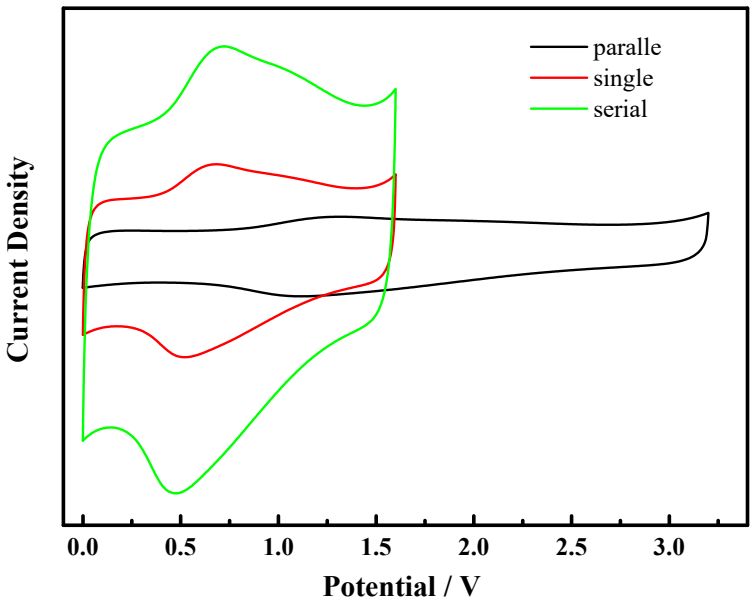

Fig. S13. CV curves of up to two AFSCs connected in parallel and in series.

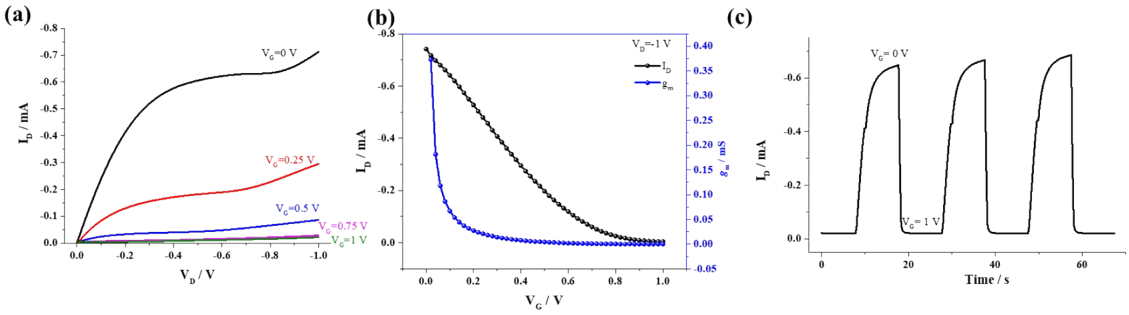

Fig. S14. Planar OECT based on PEDOT:PSS. PEDOT:PSS solution were spin coated on interdigitated microelectrode (IDME). 1 M H_2SO_4 as electrolyte and Ag/AgCl as gate (G). a) Output characteristics of a PEDOT:PSS-based OECT showing the drain-source current I_D with respect to the drain-source voltage V_D. The gate voltage V_G was varied from 0 to 1.0 V. b) Transfer characteristics of the same device and the corresponding transconductance (g_m) values at V_D = -1 V. c) Corresponding transient characteristics showing I_D as a function of time t during repeated switching of V_G between 0 and 1.0 V.

Table S1. Comparison of reported electrochemical performance of fibers based on 2D nanomaterials.

electrode	Fabrication method	electrolyte	C_v / F cm^{-3}	C_g / F g^{-1}	Ref.
$Ti_3C_2T_z$/rGO	Wet spinning	1 M H_2SO_4	341	257	1
$Ti_3C_2T_z$ /PEDOT:PSS	Wet spinning	1 M H_2SO_4	615	258	2
RGO/PEDOT:PSS	Wet spinning	PVA/ H_3PO_4	143	63.1	3
Neat $Ti_3C_2T_z$	Wet spinning	1 M H_2SO_4	1265	393	4
$Ti_3C_2T_z$ /carbon fiber	Electrospinning	1 M H_2SO_4	N/A	110	5
$Ti_3C_2T_z$ /CNT	Electrospinning	1 M H_2SO_4	N/A	100	6
Graphene/MoS_2	hydrothermal	PVA/ H_3PO_4	368	248	7
CNT/Graphene/PANI	Wet spinning	PVA/H_3PO_4	273.7	226	8
$Mo_{1.33}C$/PEDOT:PSS	spinning	3 M H_2SO_4	N/A	457	This work

Table S2. The fitting result of the element.

Element	Before cycle	After cycle
R1/Ω	13.3	14.4
R2/Ω	26.1	26.3
C2/F	6.6E-06	9.0E-06
Q2/Fs^(a^{-1})	0.0168	0.0158
a2	0.41	0.38

Reference:

[1] S. Seyedin, E. R. S. Yanza, J. M. Razal, *J. Mater. Chem. A* **2017**, *5*, 24076.

[2] J. Zhang, S. Seyedin, S. Qin, Z. Wang, S. Moradi, F. Yang, P. A. Lynch, W. Yang, J. Liu, X. Wang, J. M. Razal, *Small* **2019**, *15*, 1804732.

[3] G. Qu, J. Cheng, X. Li, D. Yuan, P. Chen, X. Chen, B. Wang, H. Peng, *Adv. Mater.* **2016**, *28*, 3646.

[4] J. Zhang, S. Uzun, S. Seyedin, P. A. Lynch, B. Akuzum, Z. Wang, S. Qin, M. Alhabeb, C. E. Shuck, W. Lei, E. C. Kumbur, W. Yang, X. Wang, G. Dion, J. M. Razal, Y. Gogotsi, *ACS Cent. Sci.* **2020**, *6*, 254.

[5] A. S. Levitt, M. Alhabeb, C. B. Hatter, A. Sarycheva, G. Dion, Y. Gogotsi, J. *Mater. Chem. A* **2019**, *7*, 269.
[6] Z. Zhou, W. Panatdasirisuk, T. S. Mathis, B. Anasori, C. Lu, X. Zhang, Z. Liao, Y. Gogotsi, S. Yang, *Nanoscale* **2018**, *10*, 6005.
[7] B. Wang, Q. Wu, H. Sun, J. Zhang, J. Ren, Y. Luo, M. Wang, H. Peng, *J. Mater. Chem. A* **2017**, *5*, 925.
[8] Z. Lu, J. Foroughi, C. Wang, H. Long, G. G. Wallace, *Adv. Energy Mater.* **2018**, *8*, 1702047.